Damage Monitoring in Composite Stiffened Skin Using Fiber Bragg Grating under Tensile and Three-Point Loading

Agus Trilaksono[1], Naoyuki Watanabe[1], Hikaru Hoshi[1], Atsushi Kondo[1], Yutaka Iwahori[2] and Shinichi Takeda[2]

1. Department of Aerospace Engineering, Tokyo Metropolitan University, Tokyo 191-0065, Japan

2. Composite Technology Centre, Japan Aerospace Exploration Agency, Tokyo 181-0015, Japan

Abstract: One of the problems associated with loading a fully composite structure with joints is that the loads are not linear through the neutral axis of the structure but are collinear; this induces additional moment and creates a load in the normal direction, which is typically a critical load because it can create delamination and can only be withstood if it is small. Another problem is that the structure is difficult to inspect using conventional methods because of limited accessibility. With fiber Bragg grating (FBG), the problem can potentially be solved in structures with a stiffness mismatch. The model used to represent the problem above is a composite stiffened skin with two loading cases: tensile and three-point bending. Additionally, FBG is used to monitor and characterize the delamination caused by both loading cases. Finite element modeling (FEM) with traction versus separation theory is performed to determine the critical area on the specimen for placement of the FBG before manufacturing and testing. In this research, FBG can successfully monitor and characterize delamination caused by both loading cases in structures that have mismatched stiffnesses. Also, FBG can predict the delamination growth quantitatively. A spectrum graph of the FBG results can be used to replace a conventional mechanical graph for use in structural health monitoring.

Key words: Carbon fiber, composite structural health monitoring, delamination, joints/joining, smart structure.

1. Introduction

In terms of design, for almost all modern aircraft, the same considerations are made when selecting the materials used to build the aircraft structure: a strong structural design and light weight. For this, composites are often the best choice. In the decades ahead, there will be one additional requirement in the design of modern aircraft: smart materials. By applying the concept of smart structures, one can expect a decrease in structural weight and maintenance efforts. Structural health monitoring (SHM) is one of the main contributions to smart structures, the concept of which is to imitate the human neural network as shown in Fig.

1. SHM is a new and alternative way of non-destructive inspection that can evaluate the integrity of the structure in real time. Also, it is important to apply SHM technology in complex structures that have limited accessibility for inspections [1-8]. For example, a structure that has a stiffness mismatch has a high possibility to create a secondary bending moment on the edge of the stiffener, which has the potential to induce a delamination failure; this is highly dependent on the magnitude of the eccentricity and the flexural rigidity of the joint because the load transfer is not collinear through the mismatched-stiffness joint but is offset or eccentric [9-10].

With fiber Bragg grating (FBG), the problem can potentially be solved. The basic principle in the operation of an FBG is described as follows. The Bragg

Corresponding author: Agus Trilaksono, researcher, research field: aerospace composite materials and structure. E-mail: trilaksono-agus@sd.tmu.ac.jp.

Fig. 1   Human neural network concept in structural health monitoring of aircraft structure.

Fig. 2   Fiber Bragg grating optical sensors principle illustration.

wavelength or reflected wavelength (λ_B) is defined by Fresnel reflection according to the following relationships:

$$\lambda_B = 2\Pi\nabla \qquad (1)$$

$$\Delta\lambda/\lambda_B = (1 - p)(\epsilon_m + \alpha_c\Delta T) + \alpha_{fo}\Delta T \qquad (2)$$

where Π is the effective refractive index of the grating in the fiber core, and ∇ is the grating period [1]. Also, $\Delta\lambda$ = wavelength shift, λ_B = base wavelength at test start, p = photoelastic coefficient (p = 0.22), ϵ_m = mechanical strain, ΔT = temperature change in K, α_c = coefficient of thermal expansion of composite, α_{fo} = coefficient of thermal expansion of fiber optic.

Fig. 2 shows each time light in the fiber encounter the FBG's refractive index discontinuities, it reflects very slightly to the spectrum analyzer and a tensile strain stretches the FBG which it increases its period, ∇. Therefore, tensile strain also increases λ_{Bragg}. That is the FBG work principles. One of the problems with implementing FBG in composite structures and materials is that it is never guaranteed that a failure will occur close enough to an FBG location to allow for strain transfer and thus have the potential to be used for fault detection and interpretation. Finite element methods with traction versus separation theory will be used, as it is the best theory for analyzing the onset of delamination at the interface between a stiffener and the skin and to plan and assure that the FBG sensors can detect damage in the right place and the right position before manufacturing and testing the specimens [11-15].

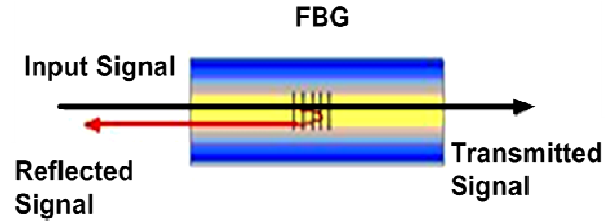This research proposes to characterize the damage of structures with mismatched stiffnesses simplified in the form of a composite stiffened skin specimen using fiber Bragg grating (FBG) strain sensors under tensile and three-point bending loads. Two loading cases are used to look for the most critical loads within structures that have mismatched stiffnesses. The paper is organized as follows: Section 2 introduces the specimen and configuration; section 3 discusses the FEM analysis verification; section 4 introduces the test setup and procedure; section 5 presents the discussion; section 6 gives conclusions.

2. Specimen and Configuration

Carbon/epoxy was used for the specimen because of its light weight, high strength, high stiffness, and corrosion resistance. Unidirectional IMS600/#133 prepreg was used in an eight-layer anisotropic stacking sequence [0, 0, 45,-45]$_s$, and it was cured in an autoclave at 180 °C. The mechanical properties of the prepreg are as follows: σ_t = 2201 MPa, σ_c = 1037 MPa, τ_t = 207 MPa, E_t = 150 GPa, E_c = 137 GPa, G_{tc} = 10.9 GPa, and v_{tc} = 0.33.

As mentioned in the previous section, Fig. 3 shows that the specimen model configuration will have mismatched stiffnesses, and as a simplification, a composite stiffened skin specimen is used. After finite element modelling (FEM) verification is performed, the FBG is embedded at the interface between the composite skin and stiffener with DP420 Off-White adhesive from 3M using the double-stage bonding method. The mechanical properties of the adhesive are as follows: τ_s = 20 MPa, τ_n = 17 MPa, τ_t = 207 MPa, and E_t = 2000 MPa. FBG made by Fujikura Fiber Optic with Ø 125 µm and a grating span of 15 mm is used for this research.

3. FEM Analysis Verification

This section deals with the quality of the composite stiffened skin using 3D modeling techniques available in Abaqus and its verification through correlation with experimental data. Several models will be proposed to get the best mechanical behavior at the edge of the composite stiffened skin.

Finite element analysis is performed before the specimen is built to verify the mechanical behavior and to determine the best position for the FBG to be installed. Traction versus separation theory will be used to verify the mechanical behavior and to predict the onset of delamination and the position at the edge region of the stiffener.

3.1 Traction versus Separation Laws

Delamination is one of the main modes of failure in composites when there is no reinforcement in the thickness direction. Delaminations can be calculated using cohesive elements, which combine aspects of strength analysis to predict the onset of damage at the interface and fracture mechanics to predict the propagation of the delamination. Cohesive elements have been found useful in the study of fractures along the interfaces of contact materials that have the same stiffness or thickness.

The cohesive constitutive law correlates the traction σ to the displacement δ at the interface. The bilinear softening model is chosen here for its simplicity. One characteristic of all softening models is that the cohesive zone can still transfer load after the onset of damage as shown in Fig. 4. For pure modes I, II, or III loading, after the interfacial normal or shear tractions reach their particular interlaminar tensile or shear strengths, the stiffnesses are gradually reduced to zero. The areas under the traction-displacement curves represent the respective (modes I, II, or III) fracture energy.

The penalty stiffness K is an arbitrarily large number selected such that the presence of undamaged cohesive elements does not introduce substantial compliance to
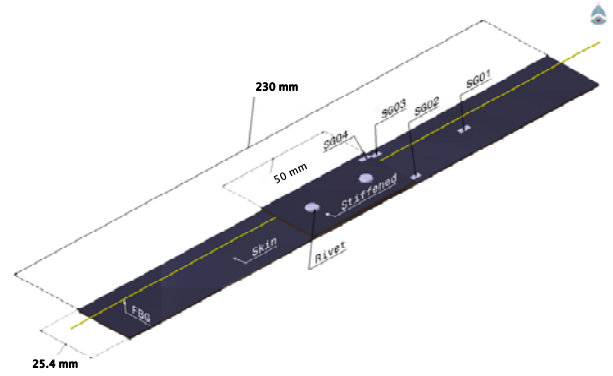

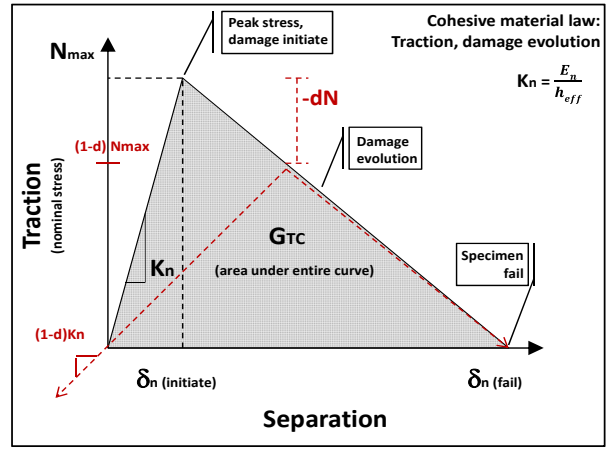Fig. 3 Specimen dimensions and configuration.

Fig. 4 Damage initiation and specimen failure based on traction vs. separation theory.

the structure. The cohesive law assumes three fracture modes. It is assumed that the 3 direction is normal to the interface and that the interlaminar shear strength δ_{shear} is independent of the shearing direction. Then, the displacement for damage initiation in each mode is simplified by the equations below.

$$\text{Mode I: } \delta_3^0 = \frac{\sigma_3^0}{K}$$
$$\text{Mode II: } \delta_2^0 = \frac{\tau_2^0}{K}$$
$$\text{Mode III: } \delta_1^0 = \frac{\tau_1^0}{K}$$

The constitutive response of traction vs. separation theory used here is based on the maximum stress criterion and is described as follows:

$$\text{MAX } \left\{ \frac{\sigma_n}{N_{max}}, \frac{\sigma_t}{T_{max}}, \frac{\sigma_s}{S_{max}} \right\}$$

Quadratic stress interaction criterion:

$$(\sigma_n) = \begin{cases} \sigma_n \text{ for } \sigma_n > 0 \\ \\ 0 \text{ for } \sigma_n < 0 \end{cases}$$

$$\left\{\frac{\sigma_n}{(N_{max})^2} + \frac{\sigma_t}{(T_{max})^2} + \frac{\sigma_s}{(S_{max})^2}\right\} = 1$$

Note: σ_n = nominal stress in the normal direction; σ_t = nominal stress in the first shear direction; σ_s = nominal stress in the second direction; d = scalar damage variable (d = 0—no damage, d = 1—fully damaged).

3.2 3D Modelling

3D modelling for this model used continuum shells for anisotropic materials and cohesive elements for isotropic materials, while shell-composite and cohesive elements were used to create the section. The contact method used between the stiffener and the skin was merging the nodes/geometry to assure that the displacement and rotation degrees of freedom were tied together for the entire node. The MAXE and QUADS damage initiation criteria were used. Damage evolution is defined based on either the effective displacement or energy dissipated. Each damage model is verified for damage in pure normal and two pure shear modes (one shear mode for two-dimensional and axisymmetric elements). Degradation of the response of the cohesive surfaces begins when the specified damage initiation criterion is met. A total of 197,990 nodes were used in the entire model.

4. Test Setup and Procedure

A static tension test on an Instron 8802 with a crosshead speed 0.5 mm/mm is conducted, and an Advanced Video Extensometer (AVE) is used to monitor the strain behavior on the back side of the stiffened area. In the three-point bending tests, the specimen is placed on a support span, and the load is applied to the center of the specimen at a specified rate with a loading nose. The test is stopped when the specimen reaches 5% displacement or if the specimen breaks before 5% (according to ISO 178). If the specimen does not break, the test is continued as far possible, and the stress at 3.5% (conventional displacement is reported.

During the static test, the optical fiber was lighted using a broadband light source (ASE FL7002, 1530-1610 nm, made by FiberLabs). The spectrum reflection was measured using an optical spectrum analyzer (MS9710C by Anritsu Co.), and the spectrum data were retrieved by a PC using the LabVIEW software from National Instruments. The spectrum reflection was continuously measured until the specimen broke.

5. Discussion

Fig. 5 shows the mesh of the merged geometry and nodes for interaction between parts. By merging the geometry and nodes, a dissimilar surface region can be avoided. The rotation and displacement degrees of freedom at the nodes are merged or tied together. The nodes are juxtaposed, and the mesh has a very good shape.

Fig. 6 shows the stress distribution in the thickness direction between the outer ply and inner ply, which were defined using the composite lay-up to create the section. This means that the 3D modelling technique used to analyse the model has the possibility to not be accurate by showing different values of stress magnitude on the outer and inner plies.

Fig. 7 shows that by using shell-composite to generate the section for this model, the correct stress distribution between the outer and inner layers is presented. Therefore, for the rest of this research, this technique will be used to build the 3D model of the composite stiffened skin.

Fig. 8 shows the maximum stress principle's vector in the normal direction. The mismatched structure clearly can be verified virtually and proves that having a loading response on the edge stiffener with stresses in the normal direction can produce a secondary bending moment, which can then have the potential to create a peeling failure. The problem is that only a small load is needed to initiate a peeling failure at the interface between the stiffener and the skin.
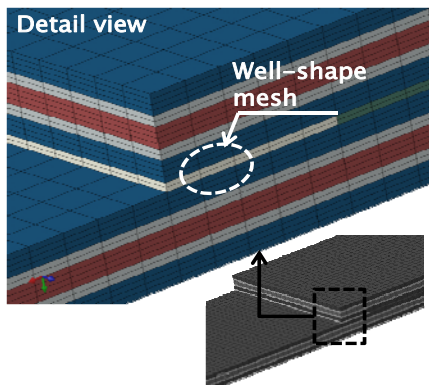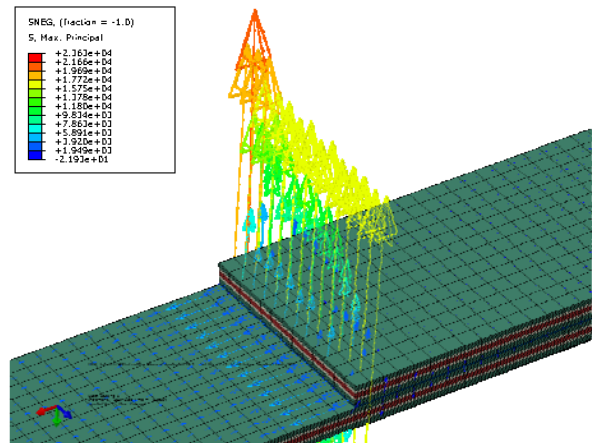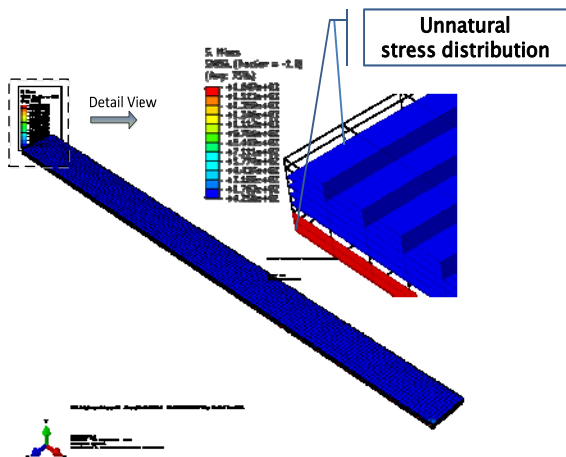
Fig. 5 Merged node interaction between parts.

Fig. 6 Composite layup used to generate the section.
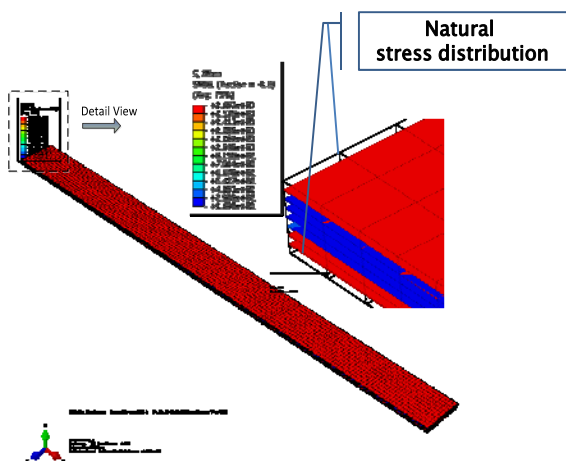
Fig. 7 Shell-composite used to generate the section.

Fig. 8 Maximum principal stress vectors in the normal direction.

delamination process compared with the normal direction load response, which is induced from the secondary bending moment at the edge of the stiffener.

Fig. 10 shows the stress concentration at the interface between the stiffener and the skin when using cohesive elements. Using this theory, it can be verified and proved that delamination onset will occur at the edge of the stiffener and will grow at that location by creating a stress concentration at the edge of the stiffened area. No out-of-plane behavior is seen in this virtual model because the element based on traction separation is a shell, which does not consider the normal direction behavior, except as shown by the vector stress response.

Fig. 11 shows the mechanical behavior magnitude from the finite element analysis in the out-of-plane direction and the extensional direction. The mechanical behaviors of straingage1 (SG1) through strain gage4 (SG4) have the same trend as the experimental results. SG4 also shows the out-of-plane behavior, which created peel and caused delamination at the edge of the stiffener. This means that there is good agreement in the mechanical behavior trend between the finite element analysis and experiment.

After FEM verification is used to determine the failure scenario and the critical position for the FBG location on the composite stiffened skin specimen, then the specimen is ready to be built and tested using the Instron 8802 machine as shown in Fig. 12. The test will

Fig. 9 virtually proves that besides a loading response in the normal direction of the structure that has mismatched stiffnesses on the edge, the created shearing load at the interface of the stiffener and the skin is a result of the deflection behavior. However, this shearing load response is less critical in the
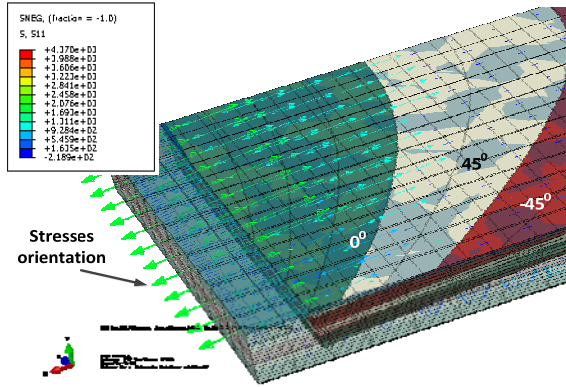
Fig. 9   Stress orientation on through-thickness section of the stiffened area.
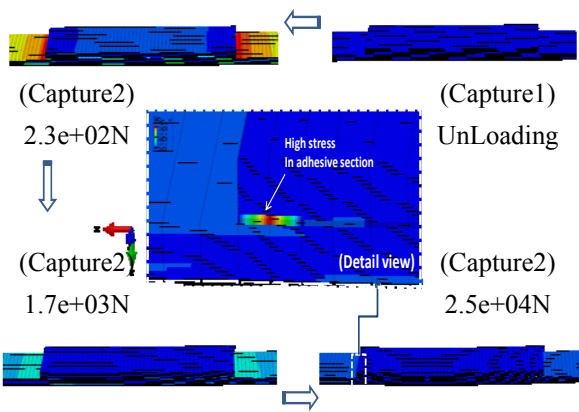

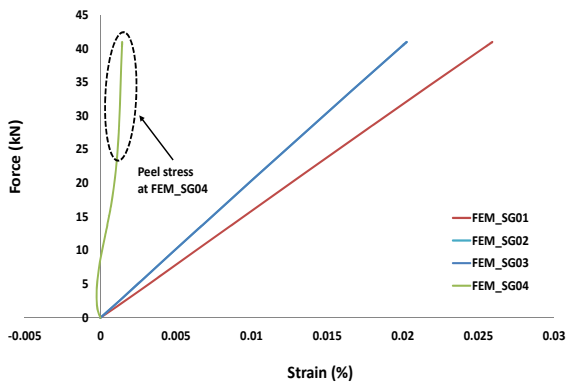**Fig. 10   Onset of delamination at edge of stiffener using cohesive elements.**

Fig. 11   Mechanical behavior based on FEM strain gage measurement.

be conducted in two steps. First, the profiling spectrum from zero loading until the specimen breaks is evaluated to obtain the complete spectrum behavior based on the FBG reading. Then, an interrupted test is conducted to determine the loaded/unloaded spectrum and the growth of delamination. After the loaded/unloaded test, the specimen is evaluated using a

Fig. 12   Tensile test setup.

C-scan machine to determine the shape of the delamination growth.

Fig. 13 shows the cut section of the specimen and C-scan result for the specimen before loading. The adhesive used to join the composite skin and stiffener has a thickness equivalent to the diameter of the FBG. Also, the blue color in the result of the C-scan before the specimen was tested indicates that the bonding between the composite skin and stiffener was perfect.

Fig. 14 shows the same tendency for the strain trend as shown in the FEM result. Strain gage SG1 through strain gage SG3 have linear strain responses, but for strain gage SG4 (top surface of stiffener), the data shows out-of-plane stresses, which are created from the peeling/opening reaction on the edge of the stiffener as the moment is reacted.

Fig. 15 shows the characteristic spectrum evolution in the bonded stiffened skin specimen from the FBG reading. There are two dominant peaks in the spectrum from the FBG readings during the given loading in the specimen, and those two peaks changed as the delamination progressed. The two dominant peaks in the spectrum are defined as P_{fp} (first peak) and P_{sp}
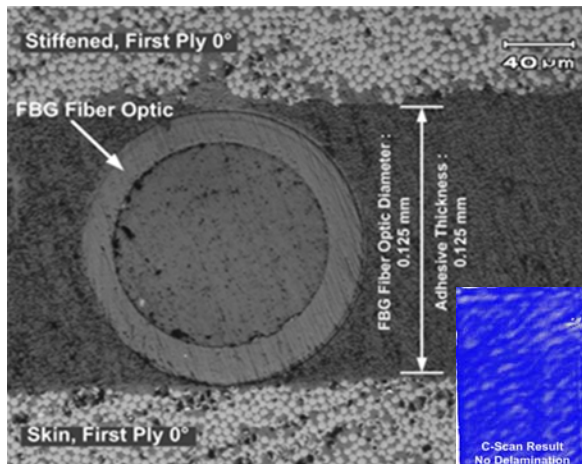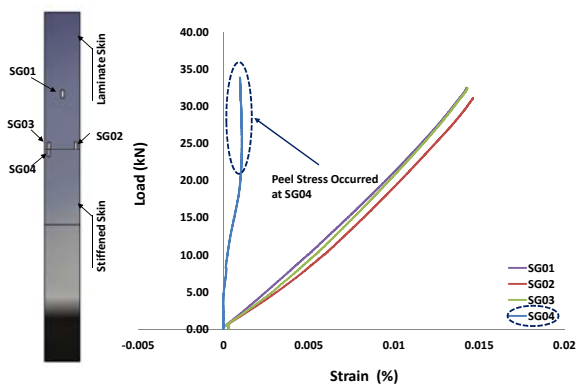
Fig. 13   Specimen cut section.

Fig. 14   Mechanical behavior based on experimental strain gage measurement.

(second peak). The two peaks in this spectrum have a value ratio (P_{fp}/P_{sp}) that is relatively linear, so it can be used to indicate the growth of delamination.

Fig. 16 shows the characteristic spectrum evolution with a change in wavelength without multiple peak occurrences. Under three-point bending, the spectrum peak has almost the same value, and only the wavelength is broader. Also, the ratio between the original wavelength and the loaded wavelength are then used to quantify the damage growth. The original and loaded wavelengths of this spectrum have a value ratio ($\Delta_{loaded} - \Delta_{original}$) that is relatively linear, so it can be used to indicate the growth of delamination.

Figs. 17a-17b shows the composite stiffened skin test result from the three-point bending test. These graphs explain that the normalized intensity could not be used as a precept of damage growth because the normalized intensity value remains almost the same
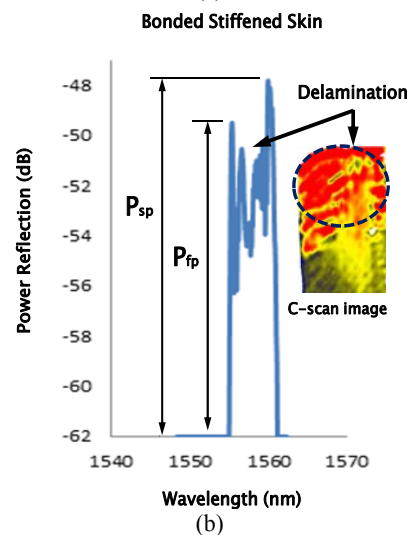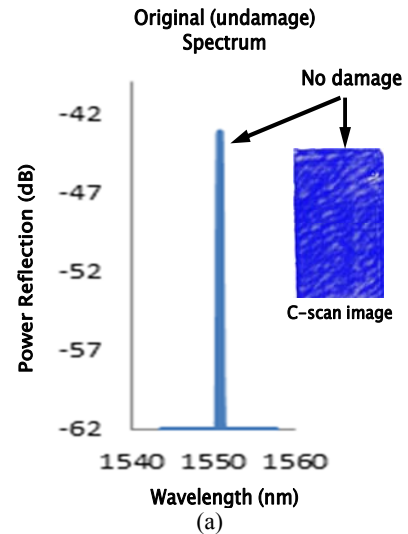

Fig. 15   Spectrum pattern from FBG reading in composite stiffened skin under tensile load: (a) Spectrum when the damage occurs; (b) Spectrum when the damage continues to grow.
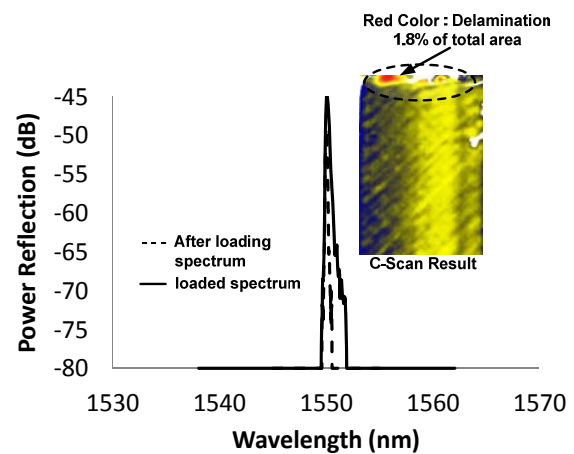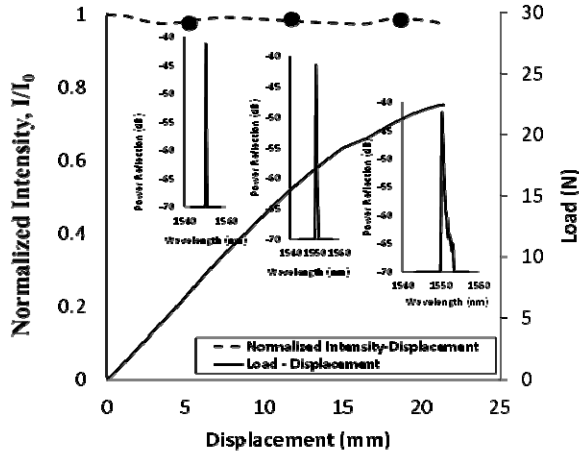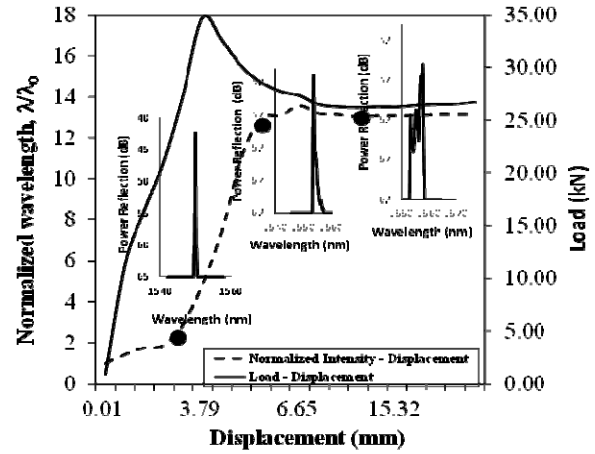

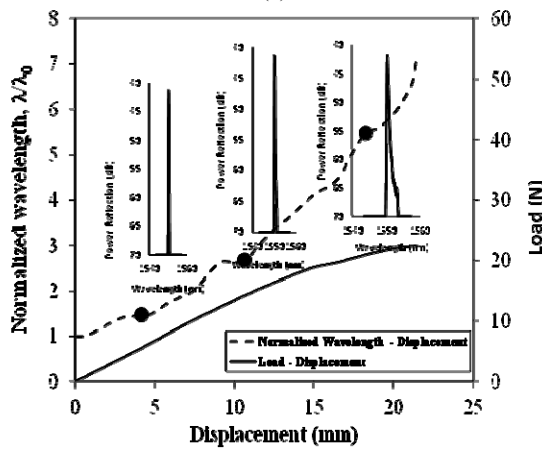**Fig. 16   After loading and loaded spectrum pattern under three-point bending load.**

(a)

(b)

Fig. 17   The relationship between normalized intensity and normalized wavelength during a loading run for the composite stiffened skin during the three-point bending test.
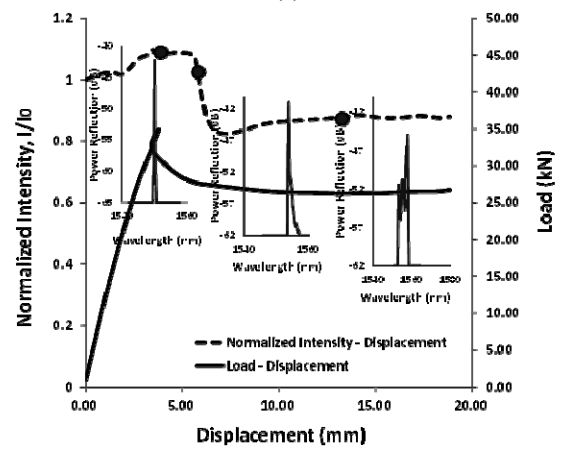

(a)

(b)

Fig. 18   The relationship between the normalized intensity and normalized wavelength during a loading run for a composite stiffened skin during the tensile test.

during a loading run. There is typically a uniform strain response in the FBG reading, but the normalized wavelength during the loading run can be used as an indication of damage growth. It was also shown that the wavelength was constantly broad compared with the original spectrum shape. After damage occurred, the normalized wavelength curve increased significantly while the load increased. This means that the normalized wavelength can be used to quantitatively measure damage in a uniform strain failure.

Figs. 18a-18b depicts the composite stiffened skin test result after the tensile test. After concentrating the load in the stiffener area, all of the loads are covered with the adhesive in the joint area, and then the peeling mode failure begins. This was indicated by the absence of an increase in load, but the displacement increased

until the specimen broke. The spectrum shape was also broad and changed significantly, and this indicated that damage occurred. After the load became constant, the shape of the spectrum reflection did not change until the specimen broke.

Figs. 19 and 20a-20b depict curve comparisons for the normalized power reflection and wavelength under tension and three-point bending. In these cases, testing under a tensile load showed the damage to grow faster than under a three-point bending load. This can be seen from the increased/decreased values on the graph normalized in the spectrum reflection and in the wavelength. This indicates that the critical load in a composite stiffened skin is in the normal direction, which creates a peeling failure. This also was clearly based on the spectrum pattern change that was
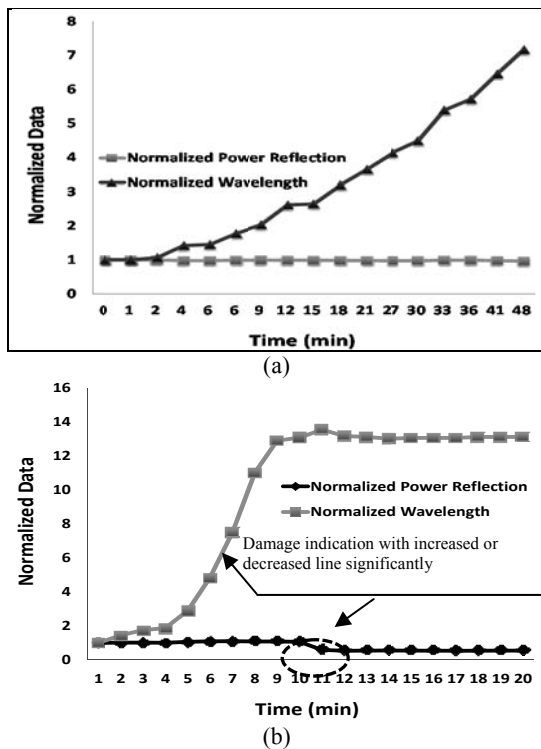
(a)

(b)

Fig. 19 Damage indication with increase or decrease in value of normalized data under tensile and three-point bending loads.
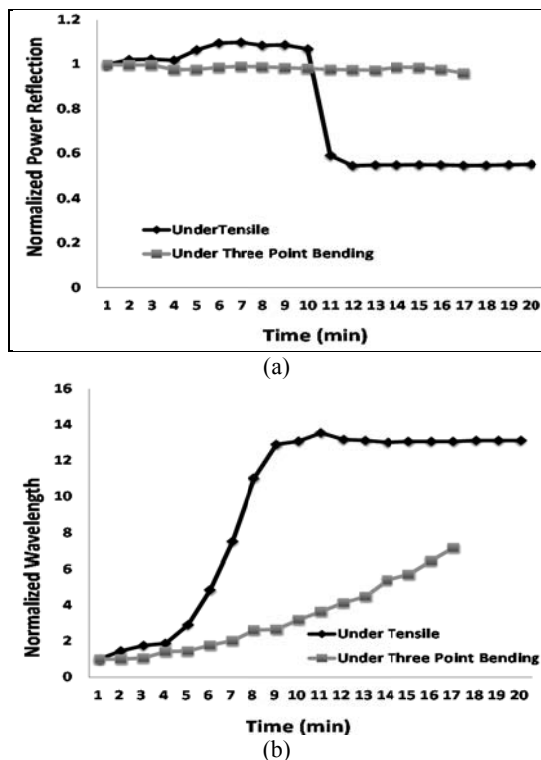

(a)

(b)

Fig. 20 Curve comparison for normalized power reflection and wavelength of the composite stiffened skin under tensile and three-point bending loads.

generated since changes in the graph line indicate the occurrence of damage. For the normalized power reflection under three-point bending, there is almost no change in the line or slope. This also indicates that the normalized power reflection under three-point bending cannot be used for damage growth prediction, but for the normalized wavelength, there is still the possibility to use it to indicate damage growth.

Figs. 21a-21b shows the interrupted loading test comparison between tension and three-point bending. The interrupted test was performed to approximate the actual conditions in the operating aircraft structure and to determine the damage growth when the structure is loaded again for FBG reading. After the interrupted test is performed, the specimen is inspected for damage using an ultrasonic C-scan. Also, only half of the stiffener area was inspected to overcome the limited capability of the ultrasonic C-scan to detect warpage in the specimen after testing. From the tensile test, the location selection from the load interrupted testis determined when the reflection spectrum shape changes, which indicates damage initiation or damage growth. In the interrupted test, the spectrum shape changes during the loading-unloading conditions, and the growth of the damage taken from the C-scan in the response spectrum of the behavior is used to quantify the damage. The sloping line shows that adhesive failure started. The load is almost constant in this phase since the peeling failure characteristic is created by the secondary bending moment phenomena. However, under three-point bending, the delamination does not grow rapidly because the load generates only shear, which is different from the tensile loading, where peeling also occurs and is a critical load on this structure.

Figs. 22a-22b shows the ratio (P_{fp} - P_{sp}) in relation to the delamination growth in the composite stiffened skin specimen, where quantification for the tensile test is obtained by referring to the ratio of the difference between value of P_{fp} and value of P_{sp} and is then compared with the trend of the delamination size as the
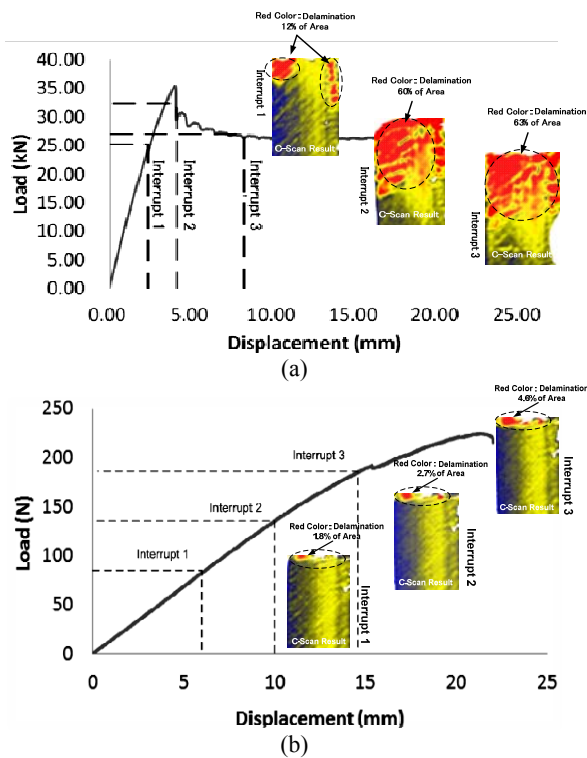
Fig. 21   Interrupted loading test comparison under tension and three-point bending.
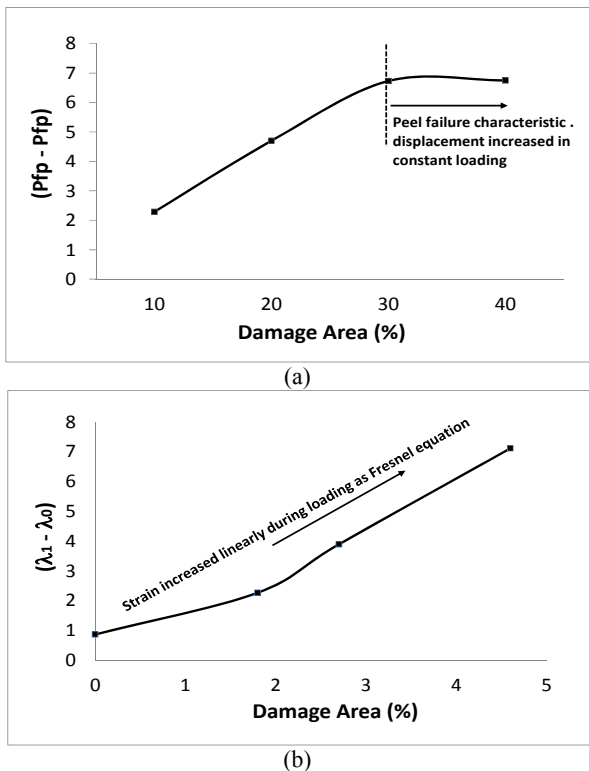

Fig. 22   Quantifying ratio of spectrum intensity due to the damage area of the bonded stiffened skin and riveted bonded stiffened skin.

result of the ultrasonic C-scan reading for the specimen. Meanwhile, the three-point bending test result is obtained by referring to the ratio of the difference between λ_1 and λ_0. The trend lines in the graph have some notable similarities: the curve increased in the relationship between the spectrum ratio or wavelength ratio and the damage area. The important information is that both specimens have a linear trend corresponding to the delamination size and growth in the spectrum pattern from the FBG reading.

6. Conclusions

An FBG strain sensor was inserted to characterize and interrogate the damage in a composite stiffened skin. The damage onset and growth predicted by FEM can be verified by FBG based on multiple peaks in the spectrum and a significantly broader wavelength. The FBG successfully detected and characterized the delamination caused by a normal load combined with a shearing load on the edge of the stiffener under a tensile load as well as the delamination induced by a shearing load in the specimen under a three-point bending load. The damage growth can be quantified successfully by the FBG reading through the ratio between multiple peaks occurring in the spectrum and through the differences in the wavelength ratios. Based on the C-scan data, it was shown that a normal direction load caused by a mismatch in stiffness like that demonstrated in the tensile test becomes more critical compared with the shearing load from the three-point bending test.

For future research, it is important to develop a combination of tensile and three-point bending loads by using an additional actuator attached to the Instron machine to create the bending load while running the tensile test on the machine. This is because in the real structure, there is never just one loading case.

References

[1] S. Takeda, Y. Okabe, T. Yamamoto, N. Takeda, Detection of edge delamination in CFRP laminates under cyclic loading using small-diameter FBG sensors, Composite Science and Technology 6 (2003) 1885-1894.

[2] S. Huang, M.M. Ohn, M. Leblanc, R.M. Measures, Continuous arbitrary strain profile measurements with fiber Bragg grating, Smart Material and Structure 7 (2) (1998) 248-256.

[3] S. Takeda, S. Minakuchi, Y. Okabe, N. Takeda, Delamination monitoring of laminated composites subjected to low-velocity impact using small-diameter FBG sensors, Composite. Part A 36 (2005) 903-908.

[4] K. Peters, P. Pattis, J. Botsis, P. Giaccari, Experimental verification of response of embedded optical fiber Bragg grating sensors in non-homogeneous strain fields, Opt. Laser Eng. 33 (2) (2000) 107-119.

[5] H. Wang, S.L. Ogin, A.M. Thorne, G.T. Reed, Interaction between optical fibre sensors and matrix cracks in cross-ply GFRP laminates. Part 2: Crack detection, Composite Science and Technology 66 (2006) 2367-2378.

[6] N. Takeda, Characterization of microscopic damage in composite laminates and real-time monitoring by embedded optical fiber sensors, Inter. J. Fatigue 24 (2002) 281-289.

[7] S. Yashiro, N. Takeda, T. Okabe, H. Sekine, A new approach to predicting multiple damage states in composite laminates with FBG sensors, Composite Science and Technology 65 (2005) 659-667.

[8] J. Botsis, L. Humbert, F. Colpo, P. Giaccari, Embedded fiber Bragg grating sensor for internal strain measurements in polymeric materials, Optic and Lasers in Engineering 43 (2005) 491-510.

[9] J.M. Gere, S.P. Timoshenko, Mechanics of Materials, 3rd SI ed., Chapman & Hall, London, 1991.

[10] J. Schijve, Secondary Bending Moment, NLR 72036U, 1972.

[11] H.Y. Ling, K.T. Lau, L. Cheng, Z.Q. Su, Mode II fracture behavior monitoring for composite laminates using embedded fiber Bragg grating sensors, Composite Structure 76 (2006) 88-93.

[12] P.P. Camanho, C.G. Davila, M.F. de Moura, Numerical simulation of mixed-mode progressive delamination in composite materials, Journal of Composite Materials 16 (2003) 1415-1438.

[13] A. Turon, P.P. Camanho, J. Costa, C.G. Davila, A damage model for the simulation of delamination in advanced composites under variable-mode loading, Mechanics of Materials 38 (2006) 1072-1089.

[14] Q. Yang, B.N. Cox, Cohesive models for damage evolution in laminated composites, International Journal of Fracture 133 (2005) 107-137.

[15] E.D. Reedy, F.J. Mello, T.R. Guess, Modeling the initiation and growth of delaminations in composite structures, Journal of Composite Materials 31 (1997) 812-831.